Anal Bioanal Chem (2002) 374 : 581–587
DOI 10.1007/s00216-001-1185-7

SPECIAL ISSUE PAPER

H. Nickel · W. J. Quadakkers · L. Singheiser

Analysis of corrosion layers on protective coatings and high temperature materials in simulated service environments of modern power plants using SNMS, SIMS, SEM, TEM, RBS and X-ray diffraction studies

Received: 29 May 2001 / Revised: 4 October 2001 / Accepted: 15 October 2001 / Published online: 21 December 2001

Abstract In three different examples, the effects of the oxidation behaviour as well as the microstructural stability of high temperature materials and protective coatings was determined by combining the results of kinetic studies with extensive analytical investigations using, among other techniques, SNMS, SIMS, SEM, TEM, Rutherford back scattering (RBS) as well as X-ray diffraction.

1) The effect of water vapour on the oxidation behaviour of 9% Cr steels in simulated combustion gases has been determined. The effects of O_2 and H_2O content on the oxidation behaviour of 9% Cr steel in the temperature range 600–800 °C showed that in dry oxygen a protective scale was formed with an oxidation rate controlled by diffusion in the protective scale. In the presence of water vapour, after an incubation period, the scales became non-protective as a result of a change in the oxidation limiting process. The destruction of the protective scale by water vapour does not only depend on H_2O content but also on the H_2O/O_2-ratio.

2) The increase of component surface temperature in modern gas turbines leads to an enhanced oxidation attack of the blade coating. Improvements in corrosion resistance and longer lifetime thermal barrier coatings in gas turbines have been achieved by improvement of the high temperature properties of MCrAlY coatings by additions of minor alloying elements such as yttrium, silicon and titanium.

3) The use of oxide dispersion strengthened (ODS) alloys provides excellent creep resistance up to much higher temperatures than can be achieved with conventional wrought or cast alloys in combination with suitable high temperature oxidation/corrosion resistance. Investigation of the growth mechanisms of protective chromia and alumina scales were examined by a two-stage oxidation method with ^{18}O tracer. The distribution of the oxygen isotopes in the oxide scale was determined by SIMS and SNMS. The results show the positive influence of a Y_2O_3 dispersion on the oxidation resistance of the ODS alloys and its effect on growth mechanisms.

Keywords Corrosion layers · Coatings · High temperature materials · SNMS · SIMS · SEM · TEM/RBS · X-ray diffraction

Introduction

The development of modern coal-fired power generation systems with higher thermal efficiency requires the use of construction materials of higher strength and with improved resistance to the aggressive service atmospheres. The increase in the thermal efficiency of steam power plants that can be achieved by increasing the steam temperature and pressure has provided the incentive for the development of the 9% chromium steels towards improved creep rupture strength and oxidation resistance. Modern steam power plants with steam temperatures around 580 °C and pressures of 30 MPa are now achieving thermal efficiencies of around 45%. With the aim of conserving fossil fuel supplies and reducing the environmental impact resulting from emissions of CO_2, SO_2 and NO_x, further development towards even higher efficiencies is necessary [1].

In addition to the development of the conventional steam-raising plant, alternative energy supply systems, such as combined cycle plants, in which a gas turbine (fired by natural gas or gasified coal) and a steam turbine are coupled, offer the prospect of even higher thermal efficiencies, as the gas turbine inlet temperatures are 1200 °C and above [2]. This results in increased oxidation rates requiring protective coatings with higher temperature capabilities. These requirements can be fulfilled only

H. Nickel (✉) · W.J. Quadakkers · L. Singheiser
Institute of Materials and Processes for Energy Systems,
IWV-2, Research Centre Juelich GmbH
and University of Technology Aachen,
52425 Juelich, Germany
e-mail: h.nickel@fz-juelich.de

by coatings of the MCrAlY-type having high aluminium contents of at least 9–10 weight-% Al.

A further increase of turbine gas temperatures can be obtained using thermal barrier coatings (TBCs) based on yttria stabilised zirconia. One of the predominant failure mechanisms of these coatings is rapid oxidation of the MCrAlY-bond coat (BC) resulting in spallation of the alumina scale due to growth stresses or thermally induced stresses resulting from different thermal expansion coefficients of the alumina scale and the bond coat. Therefore, one of the key issues in developing reliable TBC systems, which can be used as an integrated element of the blade design, are bond coats with very low oxidation rates. This can be achieved by modifying MCrAlY-compositions, especially in respect to the exact amounts of minor elements present such as silicon, titanium and yttrium [3].

Oxide dispersion strengthened alloys (ODS) are potentially suitable construction materials for components such as high temperature heat exchangers, which are subjected to hostile service conditions, due to their unique combination of superior high temperature creep and corrosion resistance. High temperature Ni-, Co- and Fe-based alloys are strengthened by a combination of solid solution and precipitation hardening. ODS alloys contain small amounts (ca 0.5–1.0 % by mass) of a finely dispersed oxide phase (mostly yttria) which is thermodynamically much more stable than the strengthening particles, such as "gamma prime" (γ') and carbides, present in conventional high temperature alloys. The ODS alloys therefore provide excellent creep resistance combined with high temperature oxidation/corrosion resistance [4].

In the present paper the significance of surface analysis techniques, in combination with conventional characterisation methods, in studying oxidation and corrosion processes of metallic materials will be illustrated thereby using examples related to the various technical applications mentioned above. The main surface analysis techniques used are secondary ion mass spectrometry (SIMS), sputtered neutrals mass spectrometry (SNMS) and Rutherford back scattering analysis (RBS). Compared to other surface analysis methods, such as AES and XPS, the SIMS technique has the advantage that it allows the detection of various isotopes of one element thus enabling tracer studies frequently used in studying growth mechanisms of corrosion layers [5, 6, 7, 8]. However, a major problem in analysing oxide layers on metallic substrates by SIMS is the strong matrix-dependence of the ion yield, which makes SIMS depth profiles difficult to quantify [5]. Therefore, in recent years a number of modified methods, i.e. SNMS [6] and MCs^+-SIMS [7] were developed which, in most cases, allow calculation of the measured intensities as function of sputter time into concentration as function of depth to be readily performed [5, 6]. Especially in case of very thin corrosion layers, conventional SIMS, MCs^+SIMS and SNMS have the disadvantage that at the beginning of the measurement, sputter equilibrium is not fully established and consequently a reliable analysis of the uppermost part of the oxide layer is in most cases not possible [7]. In such cases, RBS has been shown be an excellent complementary method to SIMS and SNMS for obtaining a full analysis of the surface oxide and the subscale regions in the alloy.

Experimental-Results

The effect of water vapour on the oxidation behaviour of 9% Cr steels

In power plants, 9% Cr steels are being used as construction materials for piping, headers and superheater tubes. For these materials, the challenge is to find a compromise between optimum mechanical properties and corrosion resistance. Studies on the thermal oxidation in simulated combustion gases of coal fired plants have shown that under these conditions, in contrast to 12% Cr steels, 9%Cr steels possess an oxidation resistance which is far lower than in air (Fig. 1). Water vapour is responsible for the rapid oxidation in the combustion gas [9, 10, 11, 12, 13, 14].

Exposures of the 9% Cr steel(P91) were carried out at up to 10,000 h at 650 °C in simulated combustion gases consisting of: 1 vol.-% O_2, 14 vol.-% CO_2, 0.1 vol.-% SO_2, 0.01 vol.-% HCl or a water content of 7 vol.-% (in N_2). SEM analysis of samples after 250 hours of oxidation under dry N_2 gas containing 1 vol.-% O_2 showed a thin oxide layer with a thickness of about 1 µm, appearing compact and adherent. The EDX analysis revealed that the scale mainly consisted of iron, chromium and minor amounts of manganese, molybdenum and silicon (Table 1). With X-ray diffraction, only the Fe_2O_3 structure could be detected.

In the wet environments a very high oxidation rate occurred after an initial incubation period, which was a function of H_2O content. In the incubation period the kinetics showed a parabolic growth rate which was slightly higher than in the dry gas. After the incubation period the curves followed a linear rate with a rate con-

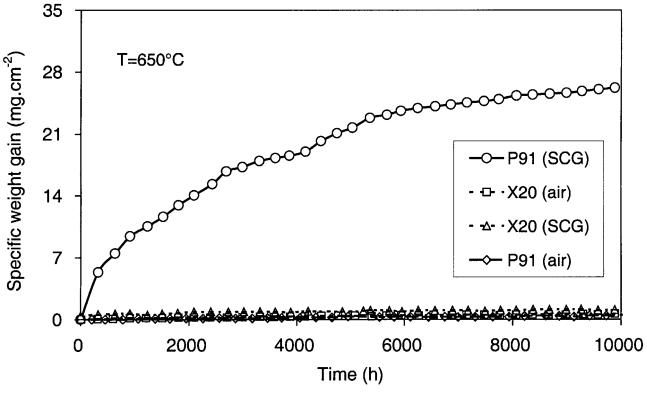

Fig. 1 Oxidation of 9% Cr (P91) and 12% Cr (X20) steels in a simulated combustion gas and air at 650 °C

Table 1 EDX analysis of scale on P91, compared with bulk alloy composition, after 250 h oxidation in N_2+1 vol.-% O_2 for 250 h at 650 °C

Element	Alloy (atom %)	Oxide layer (atom %)
Fe	88	73.2
Cr	9.6	20.4
Si	1.2	0.5
Mo	0.5	1.4
Mn	0.7	4.5

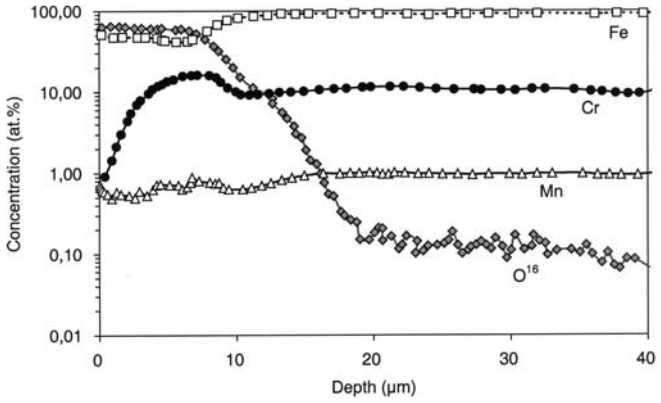

Fig. 2 SIMS profile of oxide scale (tapered cross section) of 9% Cr steel (P91) oxidised in N_2 with a 1 vol.-% O_2 +2 vol.-% H_2O mixture at 650 °C for 7 h

stant which depended on the H_2O content. The microscopic observations of the specimens oxidised in the wet gases showed porous scales which consisted of three parts, identified as Fe_2O_3 (outer), Fe_3O_4 (middle) and $(Fe,Cr)_3O_4$ (inner). This information is confirmed by the SIMS line scan, determined on a tapered cross section, which showed a chromium enrichment in the internal part of the scale, whereas no chromium was present in the outer part (Fig. 2).

The enhancement of the oxidation by the presence of water vapour does not continuously increase with temperature (Fig. 3). For 2 and 4 vol.-% of H_2O, a bell shaped temperature dependence was recorded with respective oxidation rate maxima at 650 and 700 °C. At 800 °C, however, a protective scale was formed, irrespective of the H_2O content (0, 2 and 4 vol.-%) in the gas. Consequently, at a given H_2O content of 4 vol.-% the oxidation rate in the temperature range 650–800°C decreases with increasing temperature. Results of thermogravimetric (TG) analyses at 650 °C, whereby the gas was cycled between wet and dry N_2 containing 1 vol.-% O_2 showed that when the experiment started in wet gas, the presence of water vapour rapidly led to a high rate of oxidation which was a function of both O_2 and H_2O contents with a competition between reactions at the internal interface. When the atmosphere was changed to dry, the immediate decrease of the oxidation rate can be explained to be the consequence of the new growth of an $(Fe,Cr)_2O_3$-based protective layer at the alloy/scale interface. This assumption is in good agreement with the fact that an incubation period is observed on changing the atmosphere from dry to wet.

The higher growth rate in the gas with high H_2O/O_2-ratios eventually led to a breakdown of the protective scale. This was followed by an approximately linear growth of an Fe_3O_4-rich scale. The rate of Cr incorporation into the scale was then determined by Cr diffusion in the alloy.

Corrosion resistant coatings and thermal barrier coatings of gas turbine components

Alumina scales which are formed on MCrAlY-based (M=Ni, Fe, Co) alloys or coatings can offer excellent protective capabilities due to their slow growth rate and thermodynamic stability. It is well known that minor additions of reactive elements such as yttrium improve the protective nature of the scale [15]. Also, minor silicium additions can affect the oxidation behaviour of alumina forming alloys [16, 17, 18]. Isothermal oxidation experiments of NiCrAlY alloys (with Si contents: 0–2 mass-%) at between 950 °C and 1100 °C in Ar containing 20 vol.-% O_2 showed that the growth rate of the oxide scales on Si-containing alloys were very similar to those of Si-free alloys. Cyclic oxidation at 1100 °C in air showed a similar behaviour in the early stages of oxidation. But an effect of Si became apparent after longer exposure times with better scale adherence. The results of the XRD analysis in Fig. 4 show that the oxide scales mainly consisted of α-Al_2O_3 with minor amounts of $AlYO_3$. The alloy matrix consisted of a γ-phase (Ni-solid solution), γ' (Ni_3Al), α-Cr and ß-NiAl. SNMS depth profiles revealed that after only short oxidation times Si, next to Ni and Cr, was present in the alumina scale (Fig. 5). The Si was always detected near the scale/gas interface indicating that it originated from the transient, early stages of oxidation. Si appeared to stabilise the ß-NiAl and α-Cr phase in the alloy. During cyclic oxidation, Si had a beneficial effect on oxide scale adherence and Si suppressed the formation of metastable Al_2O_3.

In another study the role of silicon and titanium on the oxidation behaviour of MCrAlY model alloys with a typical base composition, resembling that of commercial oxidation resistant MCrAlY-coatings, were produced with various additions of silicon and titanium. The base composition of the MCrAlY was Ni-20Cr-10Al-0.4Y. The silicon and titanium contents were varied between 0.4 and 2 mass-%. Oxidation kinetics were determined by isothermal gravimetry in a Setaram microbalance at temperatures between 950 °C and 1100 °C for up to 200 hours.

For the silicon and titanium modified coating systems, the isothermal oxidation behaviour at 1100 °C showed no significant ef-

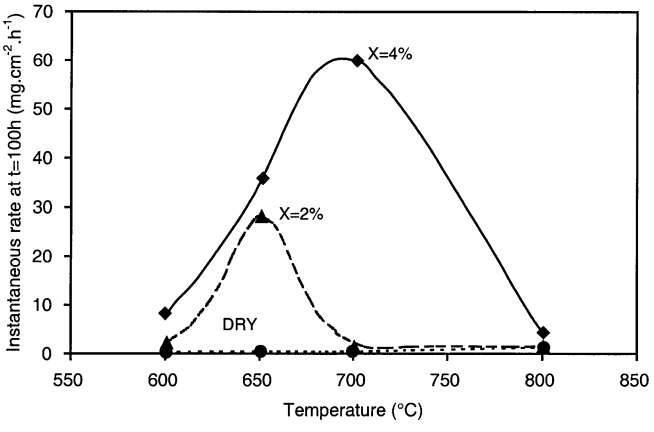

Fig. 3 Influence of water vapour on the rate of oxidation of 9% Cr steel (P91) in N_2 with 1 vol.-% O_2+x vol.-% H_2O mixtures between 600 and 800 °C

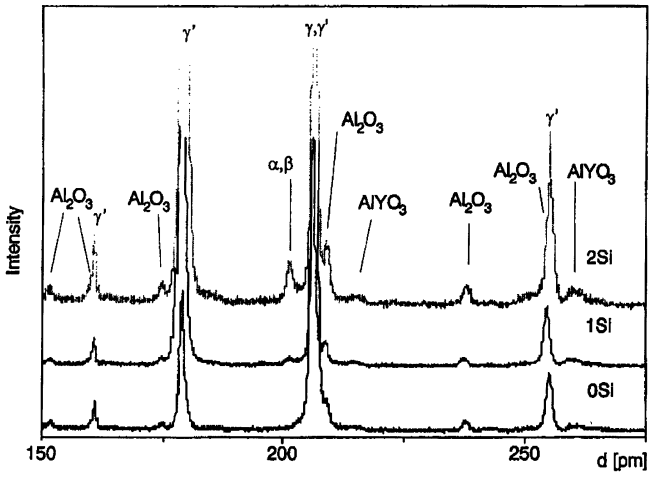

Fig. 4 X-ray diffraction results of NiCrAlY alloys with different Si contents after 200 h isothermal oxidation at 1000°C in Ar+20 vol.-% O_2

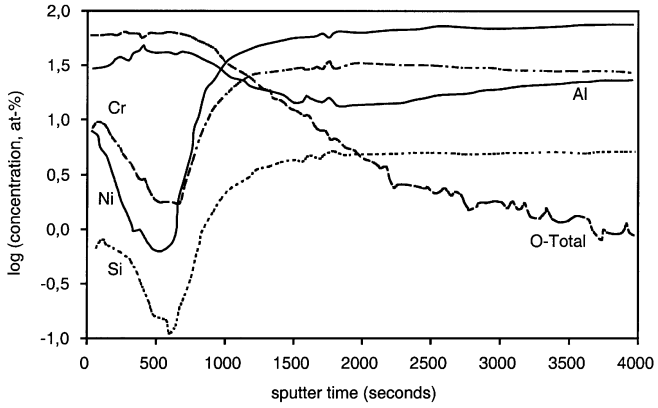

Fig. 5 SNMS depth profiles of alumina scale on NiCrAlY+2 mass.-% Si after 6 h oxidation at 1000 °C in Ar+20 vol.-% O_2

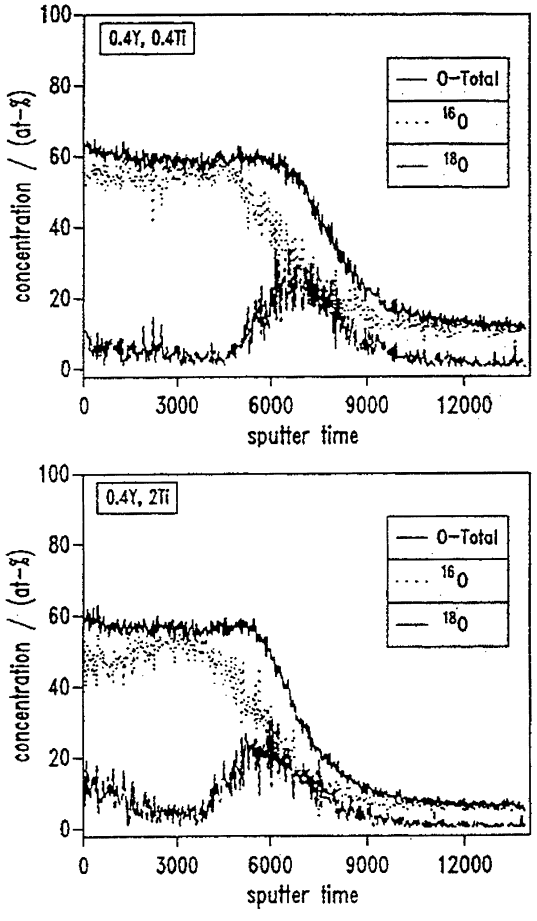

Fig. 6 Oxygen isotope distribution in alumina scales on Ni-20Cr-10Al-0.4Y with 0.4 mass.-% Ti and 2 mass.-% Ti after two-stage oxidation in air/air+$^{18}O_2$ (16 h/32 h) at 1000 °C

fect on the isothermal oxidation behaviour of silicon or titanium. However, under cyclic oxidation conditions, silicon and titanium appeared to possess a clear effect on the oxidation properties. Additions of 2 mass-% Si appeared to be beneficial in improving oxide scale adherence during thermal cycling at 1100 °C. In titanium modified coatings, low Ti concentrations (0.4 mass-%) appeared to improve oxide scale adherence, whereas for higher titanium concentrations the onset of spallation was shifted to shorter oxidation times.

Metallographic investigations revealed that titanium and silicon additions led to a significant change in the coating microstructure: in general the microstructure consisted of a NiCr matrix with low Al content (typically 4–5 mass-%), which corresponded to the γ-phase. Aluminium was enriched in the β-phase which corresponded to the intermetallic compound NiAl. Both silicon and titanium changed the morphology of the β-phase precipitates and affect precipitation of additional phases. Increased titanium content promoted the precipitation of gamma prime (γ') and α-chromium, whereas silicon additions promoted the formation of very small α-chromium particles.

Two-stage oxidation experiments were carried out to check whether silicon and/or titanium affect the alumina growth mechanisms after longer oxidation times. In the first stage, the specimens were oxidised in normal air and in the second one, a controlled amount of ^{18}O was added to the gas atmosphere without intermediate cooling. Subsequently, the localisation of the oxygen isotopes in the scale was measured by SNMS.

This two-stage oxidation technique with subsequent isotope analysis in the surface scale is a suitable technique to study the growth processes occurring in the protective oxide scales [5, 6]. It has frequently been shown [6, 8], that the technologically relevant oxide scale properties, growth rate and adherence, are strongly affected by the processes dominating the oxide scale growth, i.e. cation diffusion, anion diffusion or a combination of both processes, either proceeding through the oxide lattice or the grain boundaries.

Fig. 6 shows typical oxygen isotope profiles for Ti containing model alloys. The oxygen ^{18}O isotope is mainly concentrated at the alumina scale/MCrAlY-interface, indicating predominant growth of the scale by inward oxygen diffusion through grain boundaries, irrespective of Ti content. Similar results were found for Si-modified Ni-20Cr-10Al-0.4Y model alloy [3].

Oxide dispersion strengthened (ODS) alloys

As mentioned above oxide dispersion strengthened alloys (ODS) are subjected to service conditions due to their unique combination of superior high temperature creep and corrosion resistance.

Growth, adherence and composition of oxide scales

For their high temperature oxidation/corrosion resistance the nickel- and iron-based ODS alloys rely on the formation of slow growing and well adherent chromia and alumina scales. Examples of commercial Fe- and Ni-based ODS alloys are given in Table 2. For the determination of the oxidation behaviour, MA 754 and MA 956 were chosen as an example of chromia forming alloys and alumina forming materials, respectively. The results have been compared with those obtained for conventionally produced wrought alloys Ni-25Cr and Fe-20Cr-5Al. Fig. 7 compares the X-ray diffraction analysis of the surface scales after 300 hours of isothermal oxidation at 1000 °C in synthetic air. The ODS alloy clearly exhibited a very selective oxidation of chromium whereas the scale of Ni-25Cr contained significant amounts of $NiCr_2O_4$ and NiO in addition to chromia. Isothermal and cyclic oxidations of the alumina former MA 956 and the conventionally produced wrought

Table 2 Nominal composition of commercially available iron- and nickel-based ODS-alloys

Alloys	Composition in Mass.-%									
	Ni	Fe	Cr	Al	Ti	W	Mo	Ta	C	Y_2O_3
MA 956	–	Base	20	4.5	0.3	–	–	–	0.04	0.5
MA 754	Base	–	20	0.2	0.3	–	–	–	0.04	0.5
MA 6000	Base	–	15	4.5	2	2	2	2	0.04	1
MA 760	Base	–	20	6	–	3.5	2	–	0.04	1

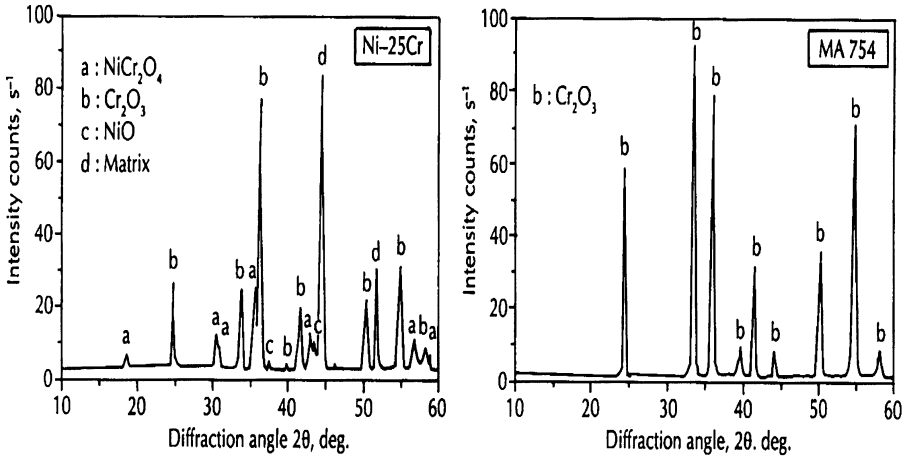

Fig. 7 X-ray diffraction results of MA 754 and Ni-25 Cr after 300 h isothermal oxidation at 1000 °C

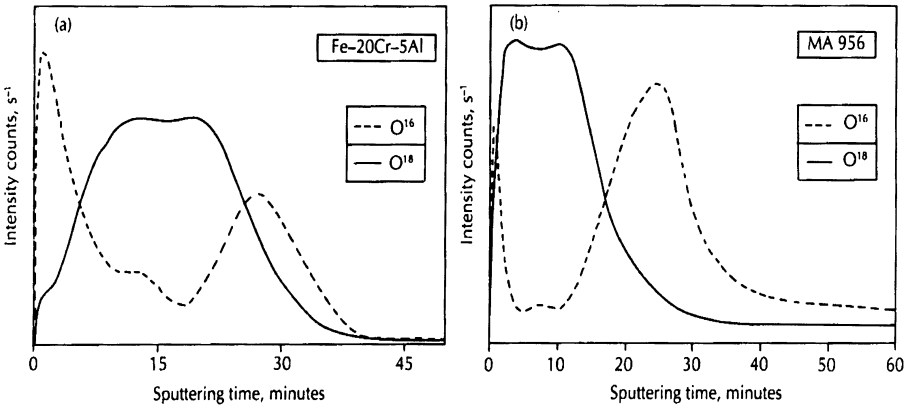

Fig. 8 Distribution of the oxygen isotopes ^{18}O and ^{16}O in the oxide layer of the aluminium oxide formers after 3 h oxidation in ^{18}O-enriched air followed by 9 h of oxidation in normal air at 1000 °C

alloy Fe-20Cr-5Al showed that the differences in oxidation behaviour between ODS- and non-ODS alloys were similar to those for the chromia formers: the spallation resistance of the scale on the ODS alloy was superior and the scale growth was slower than that on Fe-20Cr-5Al.

Investigations of the growth mechanisms of protective chromia and alumina scales

The growth mechanisms of the oxide scales were examined by a two-stage oxidation method with ^{18}O as tracer; the distribution of the oxygen isotopes in the oxide scale was determined by SIMS. From SEM measurements the scale morphology between the ODS and conventional alloys were determined. After oxidation for 8 h at 1100 °C, the scale on the conventional alloy Fe-20Cr-5Al had a convoluted surface, whereas that of the ODS alloy MA 956 was very flat with only the formation of small spherical particles apparent. Fig. 8 shows the depth profiles for the oxygen isotopes ^{18}O and ^{16}O in the oxide layer on the aluminium formers measured with SIMS after different oxidation steps in air at 1000 °C. The results show that the scales on Fe-20Cr-5Al grew by cation transport to the scale/gas interface as well as by oxygen transport to the scale-alloy interface: the ^{16}O introduced in the second oxidation stage is clearly enriched near the interface. This was also the case for the ODS alloys, however, the enrichment at the scale/gas interface, especially for MA 956 (shown), was essentially smaller than for the conventional alloy. This showed that for the ODS alloys, the cation transport was reduced and made only a small contribution to the overall oxide growth; the layer grew almost exclusively by oxygen transport. The oxidation experiments with alumina- and chromia-forming ODS alloys have demonstrated that additions of yttria decrease the oxide growth rate, improve scale adherence, and enhance selective oxidation. The addition of Y_2O_3 significantly reduces the outward growth by reducing the outward cation transport. Decreased cation transport reduces the pore formation at the scale-metal interface, as a result of vacancy condensation and thereby prevents the formation of convoluted, poorly adherent scale. SIMS imaging clearly showed that the oxygen transport occurred through localised paths in the alumina scale. Comparison with SEM studies of oxide fracture surfaces strongly indicates that the localised paths for oxygen transport are the scale grain boundaries. In the case of alloys with 0.17 mass-% and 0.7 mass-% yttria, the scale growth occurs nearly exclusively by oxygen diffusion. Only a small amount of yttrium and titanium outward diffusion occurs. Apparently, a minimum amount of yttria (>0.02 mass-%) was necessary to suppress the aluminium transport in the scale.

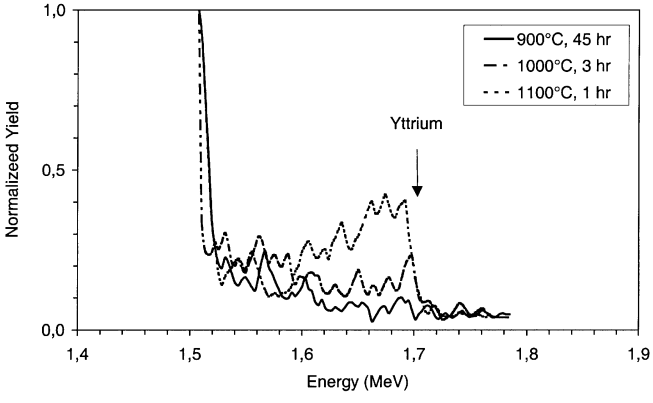

Fig. 9 RBS analysis of oxide scales on alloy MA 956 after different oxidation times in the temperature range 900–1100 °C

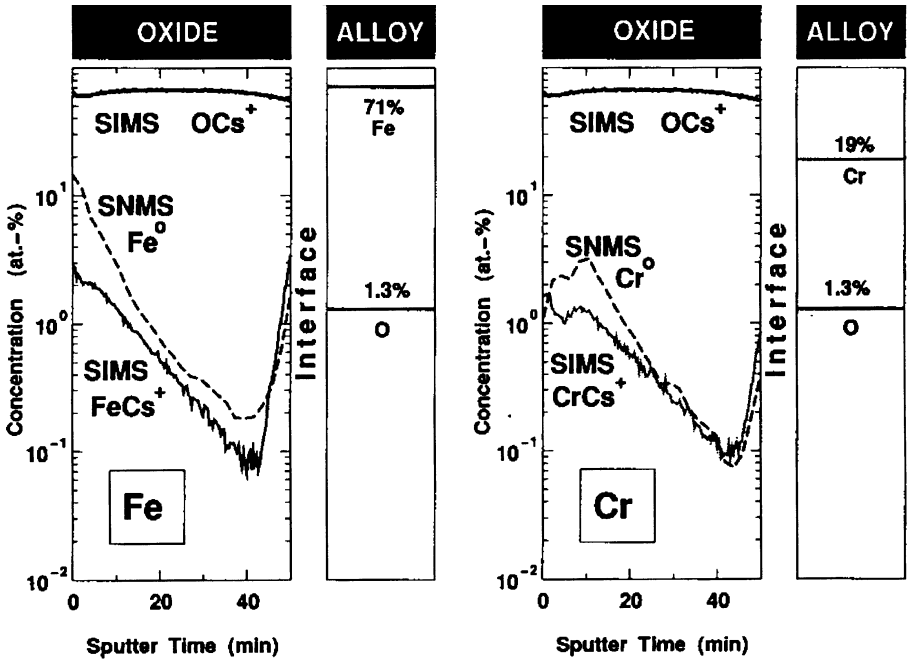

Fig. 10 Concentration profiles of Fe, Cr, and O in the oxide (alumina) film of the ODS-alloy MA 956 (containing 0.21 mass.-% Y in form of yttria dispersion) versus sputter time for MCs^+-SIMS and SNMS. The relative sensitive factors (RSFs) for the calculation of the concentration profiles have been described in [7]

Decreased transport of nickel and/or iron cations reduced spinel oxide formation and consequently selective oxidation. Detailed analysis of oxide scales by TEM has shown that yttrium tends to be enriched at the grain boundaries both in Al_2O_3 and Cr_2O_3 scales [19, 20]. Analysis of the oxide on the ODS alloy MA 956, after different oxidation times in the range 900–1000 °C, has additionally used the Rutherford backscattering (RBS) method. The results in Fig. 9 confirm that yttrium becomes concentrated at the outer surface of the oxide film.

In another study the growth mechanism of oxide films on ODS alloys have been investigated more quantitatively. In order to quantify the similarities between e-beam SNMS and MCs^+-SIMS, relative sensitivity factors (RSF) have been determined for the elements Fe, Cr, and Al from the alloy composition and compared with Fe, Cr, Al, and O from Fe/Cr-implanted sapphire [7, 21]. The published RSF factors of Quadakkers et al. [7] have shown that, particularly for MCs^+-SIMS, different RSFs have to be used for the oxide and the alloys. Fig. 10 summarises the results for Fe and Cr as measured with SNMS and MCs^+-SIMS for the ODS alloy MA 956. Good general agreement is found for the element profiles measured by the two different methods. However, for both alloys the deviations in the concentrations as calculated for the oxide show systematic trends. At low concentrations the SNMS profiles diverge from SIMS-profiles by a factor of 2; an even larger deviation occurs near the oxide surface. For Cr, the agreement between the two methods is excellent at low concentrations and only above 1 at.-% Cr is the SNMS profile a factor of 2–3 higher than the MCs^+-SIMS result. This seems to be surprising because the RSFs employed were taken from implantation concentration profiles between 0.1 and 1 at.-% and therefore a good agreement between SIMS and SNMS at least for this range of concentrations would be expected. The systematic differences between the two independent methods might be caused by the fact that the implantation standards used do not completely resemble the chemical state of the elements in the oxide film. Therefore these results do not absolutely define which of the methods yields the true concentration profiles.

Summary

Summarising, the effect of O_2 and H_2O content on the oxidation behaviour of 9% Cr steel in the temperature range 600–800 °C shows that in dry oxygen a protective scale is formed with an oxidation rate controlled by diffusion in the scale. In the presence of water vapour, the scales become non-protective, as a result of a change of the oxidation limiting process. The destruction of the protective scale by water vapour does not only depend on H_2O content but also on the H_2O/O_2-ratio. At low contents of H_2O and high contents of O_2 a slow parabolic dependence is observed with the scale growth being controlled by diffusion through a scale with a composition $(Fe,Cr)_2O_3$. At high contents of H_2O and low contents of O_2 the oxidation also initially starts with a parabolic dependence, however with a slightly higher rate than in dry gas. The oxidation rate during the first hours of oxidation is a function of the ratio H_2O/O_2, possibly as a result of the contribution of substitutional hydroxide to scale growth. The higher growth rate in the gas with high H_2O/O_2 ratios eventually leads to a breakdown of the protective scale. This is followed by an approximately linear oxidation of an Fe_3O_4-rich scale in which the rate is probably controlled by a competition of reactions between O_2 and H_2O at the internal interface.

Studies of protective alumina scales which form on NiCrAlY-alloys with Si addition show that Si concentrations up to 2 mass-% have only a minor effect on scale growth of Ni-20Cr-10Al-Y during isothermal oxidation. Si appeared to stabilise the ß-NiAl and (α-Cr-phase in the alloy and had a beneficial effect on oxide scale adherence during cyclic oxidation.

Considerable efforts have been made in the improvement of high temperature properties of MCrAlY coatings by additions of minor alloying elements such as yttrium, silicon and titanium. But the results clearly show that, for a given MCrAlY-base composition, additions of further alloying elements and their amount have to be carefully adjusted. The yttrium content of commercial coating com-

positions, which is typically between 0.5 and 1 mass-%, should be lowered to avoid internal oxidation of yttrium. Small additions of Ti and Si can improve oxide scale adherence. For titanium, the beneficial effect is only obtained for small additions around 0.4 mass-%.

The oxidation behaviours of Fe- and Ni-based oxide dispersion strengthened (ODS) alloys of the type MA 956 and MA 754 were investigated at temperatures between 900 °C and 1100 °C. The main emphasis was placed on the effect of alloy yttria content on scale composition and structure. By using SNMS and SIMS depth-profiling and SIMS imaging it was found that yttria additions to the alloy changed the transport phenomena in such a way that the scales on the ODS alloys grew nearly exclusively by oxygen grain boundary transport. TEM-studies revealed that yttria was incorporated in the scale grain boundaries as precipitations and as segregation layer. RBS measurements confirmed that yttria became concentrated at the outer surface of the oxide film during long term oxidation.

References

1. Nickel H, Ennis PJ, Quadakkers WJ (2001) Min Pro Ext Met Rev (Mineral Processing and Extractive Metallurgy) 22:181–195
2. Ennis PJ, Wachter O, Nickel H (1996) Pressure Vessels & Piping Conference (1996 PVP) and the Eighth International Conference on Pressure Vessel Technology (8-ICPVT), 21–26 July, 1996, Montréal, (Canada), ICPVT- 1: 461–466 (ASME 1996)
3. Nickel H, Clemens D, Quadakkers WJ, Singheiser L (1999) Trans ASME 121:384–387
4. Korb G (1990) In: Arzt E, Schulz L (eds) Proc Conf New Materials by Mech Alloying Techniques. DGM, Oberursel, pp 175–182
5. Quadakkers WJ, Viefhaus H (1995) In: Grabke HJ (ed) Proc in "EFC Publications"14, Guidelines for Methods of Testing and Research in High Temperature Corrosion. The Institute of Materials, London, pp 189–217
6. Quadakkers WJ, Elschner A, Speier W, Nickel H (1991) Appl Surf Sci 52:271–287
7. Pfeifer JP, Holzbrecher H, Quadakkers WJ, Speier W (1993) Fresenius J Anal Chem 346:186–191
8. P. Kofstad (1988) High Temperature Corrosion, Elsevier, London
9. Kofstad P (1991) In: Bennett MJ, Lorimer G (eds) Microscopy of oxidation. The Institute of Materials, London, pp 2–9
10. Williams C, Thiele M, Quadakkers WJ, Proceedings EUROCORR 96, Nice, France, III:10/1–10/4
11. Rahmel A, Tobolski J (1965) Corrosion J Sci 5:333–346
12. Galerie A, De Nicola MR, Pettit JP (1993) In: Newcomb SB, Bennett MJ (ed), Microscopy of oxidation. The Institute of Materials, London, pp 338–346
13. Nickel H, Wouters Y, Thiele M, Quadakkers WJ (1998) Fresenius J Anal Chem 361:540–544
14. Ehlers J, Smaardijk EJ, Penkalla HJ, Tyagi AK, Singheiser L, Quadakkers WJ, Proceedings 14. International Corrosion Congress, 26.09.–01.10.1999, Cape Town, South Africa, paper 336
15. Huntz AM (1989) In: Lang E (ed) Applied Science. Elsevier, London, pp 81–109
16. Clemens D, Vosberg VR, Hobbs LW, Breuer U, Quadakkers WJ, Nickel H (1996) Fresenius J Anal Chem 355:703–706
17. Zheng Y, Cai Y, Mo L, Yang Z (1991) J Mater Eng 13:39–46
18. Rahmel A, Schütze M (1992) Oxid Met 38:255–266
19. Quadakkers WJ (1990) Werkstoffe und Korrosion 41:659–668
20. Clemens D, Bongartz K, Speier W, Hussey RJ, Quadakkers WJ (1993) Fresenius J Anal Chem 346:318–322
21. Oechsner H (1984) In: Oechsner H (ed) Thin film and depth profile analysis, topics in current physics, Vol 37. Springer, Berlin Heidelberg New York